JOURNAL OF PROPULSION AND POWER
Vol. 22, No. 3, May–June 2006

Characterization of Dryout Point in the Vaporizing Liquid Microthruster

J. Blandino* and M. McDevitt†
Worcester Polytechnic Institute, Worcester, Massachusetts 01609
and
J. Mueller,‡ D. Bame,‡ and A. Green‡
Jet Propulsion Laboratory, California Institute of Technology, Pasadena, California 91109

A specially designed vaporizing liquid microthruster (VLM) with a Pyrex cover glass to provide optical access has been used to investigate the two-phase flow of water through the heated channel, which is approximately 700 μm wide and 300 μm deep. The design and calibration of a feed system to control mass flow to the VLM in the range of 75–250 μg/s is described along with the video microscopy system used for optical imaging of the phase transition within the channel. Images are presented showing the flow structure during the initial vapor formation, a pulsing mode of operation, and unsteady interaction between individual vapor packets within the channel. As the flow rate is increased from 135–175 μg/s at a heater power of 0.85 W, the location of phase boundary (dryout point) is found to move downstream by approximately 1 mm. Two candidate flow instabilities that could account for the observed unsteady behavior are discussed as well.

Nomenclature

D	=	tubing diameter, m
f	=	Darcy friction factor
L	=	tubing length, m
$\dot{m}$	=	mass flowrate, kg/s
Re	=	Reynolds number in supply tube
S	=	flow sensitivity factor, μg/s/psi
T	=	ambient temperature used in viscosity correction, K
T_0	=	reference temperature used in viscosity correction, K
V	=	flow mean velocity, m/s
ΔP	=	feed system pressure drop, psi
μ	=	liquid viscosity, kg/m/s
μ_0	=	liquid viscosity at a reference temperature, kg/m/s
ρ	=	liquid density, kg/m^3

Introduction

THE consideration of microspacecraft by NASA, the Air Force, and private industry in the last decade has led to a number of research activities investigating microthrusters. In this context, these are thrusters that have thrust on the order of micronewtons to millinewtons and are physically small, in some cases fabricated using techniques common in the development of microelectromechanical systems (MEMS). This is in contrast to micronewton thrusters (such as colloid and some field emission electric propulsion devices), which are designed to produce thrust in the micronewton range but are not necessarily constructed to minimize packaging volume. This latter category is intended primarily for the role of providing ultrafine position control of spacecraft.

An extensive review of thruster options for microspacecraft is provided by Mueller in Chapter 3 of Ref. 1. This reference provides detailed information on a dozen microspacecraft designs, all except one with a wet mass less than 75 kg. This reference also lists some demanding attitude control propulsive requirements for spacecraft that have a mass and moment of inertia less that 20 kg and 1 kg-m^2, respectively. Particularly challenging is the need to keep the spacecraft pointed within some angular range, from a degree down to several arcseconds over time scales of tens of seconds. This requirement usually drives the need for minimal impulse bit, whereas the need for a reasonable slew time to reorient the spacecraft can drive the steady-state thrust requirement.

One option that has been considered for this role is the pulsed plasma thruster (PPT).[1–3] Various configurations of PPTs have been considered for fine control of larger spacecraft in formations.[4–7] These studies have evaluated mission performance as well as possible impact of contamination on other spacecraft in the formation.[4,8] The vaporizing liquid microthruster (VLM) developed at the Jet Propulsion Laboratory[1,9] (JPL) represents another possible candidate for attitude control of microspacecraft. The VLM is an electrothermal thruster in which a liquid propellant is heated to vaporization and expelled through a nozzle to produce thrust. The potential role of a VLM would be as an attitude control thruster on microspacecraft. From Ref. 1, the VLM is intended to produce thrust in the range of 0.1–1.0 mN and have a minimum impulse bit capability of 10^{-7} to 10^{-5} N-s. In this role, the specific impulse is not as critical a driver as would be the case for a primary propulsion system. Thrust and flow-rate measurements made in Ref. 9 indicate a specific impulse of at least 100 s. This compares well with typical cold-gas systems (approximately 60–80 s *Isp*) and eliminates the need for the relatively massive, high-pressure storage of a gaseous propellant. In such an attitude control role, the thruster would operate in a pulsed mode producing the minimum impulse bit to maintain pointing over some angular range with minimal disturbance. For repointing slews (180 deg/min), steady-state operation at the millinewton level would be required. Tests to date have focused on water as a propellant although others that have been considered include ammonia and hydrazine.[9]

The VLM is fabricated using MEMS techniques, which have made it a candidate for some microspacecraft designs with very limited surface area available for installation. In the most recently tested versions of the VLM, a compact (but not MEMS fabricated) valve is mounted to a Pyrex thermal standoff just upstream of the heater channel inlet as shown in Fig. 1. The propellant supply capillary runs through this standoff. For a complete description of the VLM design and results of initial performance characterization tests, the reader is referred to Chapter 8 of Ref. 1.

Presented as paper 2003-4719 at the AIAA/ASME/SAE/ASEE 39th Joint Propulsion Conference and Exhibit, Huntsville, AL, 20–23 July 2003; received 18 February 2005; revision received 3 August 2005; accepted for publication 25 August 2005.

*Assistant Professor, Mechanical Engineering Department.
†Student, Mechanical Engineering Department.
‡Member of Technical Staff.

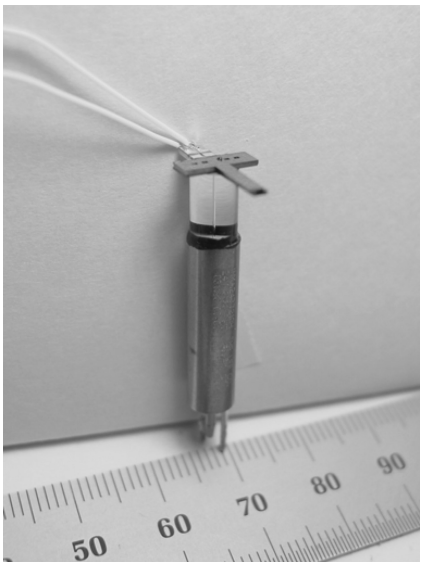

Fig. 1 VLM (from Ref. 9) integrated with Lee Corp. solenoid valve and Pyrex thermal standoff.

Other groups have also investigated variations on MEMS-fabricated, water vaporizing thrusters. Mukerjee et al.[10] designed, fabricated, and tested a vaporizing liquid microthruster in order to explore sensitivity of performance to flow rate, heater power, and inlet temperature. The device tested was an asymmetrical design fabricated with a glass cover on one side to permit observation of the flow in the channel over the heater and exiting the nozzle. The powers reported are those required to vaporize the flow that has already been heated to a specified inlet temperature. In one set of tests at a water flow rate of 0.21 ml/min (4 mg/s) and (controlled) inlet temperature of 82.5 °C, the authors reported a maximum thrust of 0.31 mN at 7.8 W. This increased to 0.46 mN at 10.8 W at a flow rate of 0.53 ml/min (9 mg/s). Of particular relevance to the present work is the measurement of vaporization point relative to channel length as a function of liquid flow rate. At a fixed power (5 W), this dryout point appears to vary smoothly with flow rate over the approximate 5 mm length of the channel as the flow is varied from 1–10 mg/s. The apparent stability of these flow conditions might have been in part caused by the control of the inlet temperature (using preheater coils).

Ye et al.[11] have investigated a variant of the MEMS-fabricated vaporizing thruster designed to operate in a pulsed mode. In one series of tests, heating was controlled by applying a 34-V pulse across a 39 Ω resistive heater at a rate of 30 Hz with a 900-μs pulse width. Although the description of the device indicates that the intention is to vaporize the water, the authors use a laser Doppler velocimeter to measure speed and size distribution of what they refer to as "ejected water vapor particles." The average velocity for this test series was measured to be 8.9 m/s with a peak velocity of 20 m/s. This velocity, and the fact that individual particles are being detected, strongly suggests the authors were observing liquid droplets. Using the flow rate measured for this test (approximately 0.025 mg/s) and the average measured particle velocity, the impulse delivered over a 1-s period was calculated to be 0.2×10^{-6} Ns. The very low specific impulse of this device, less than 1 s on average, suggests that pulsed operation is not attractive for application as a thruster unless full vaporization can be maintained.

More recently (2005), Maurya et al.[12] have fabricated a vaporizing liquid microthruster using MEMS techniques and measured thrust using water as a propellant. In one set of tests, with a flow rate of 0.7 μl/s (0.7 mg/s) the thrust varied from 25–120 μN over a heater power range of 1.1–2 W. In these tests the water was supplied at room temperature (25 °C). The authors compare their results with the earlier work of Mukerjee et al.[10] and attribute some of the differences in the results to the differences in heater design (internal vs external) and liquid inlet temperatures (25 vs 82.5 °C).

In 2003, VLM test results were reported by Mueller et al.[9] of thrust stand measurements made in a vacuum chamber at JPL using water as a propellant (device shown in Fig. 1). In one test run lasting approximately 400 s with a VLM heater power of 1.07 W, they measured a thrust ranging from 61–140 μN during which the flow rate varied between 99–140 μg/s. At this flow rate and power, the performance was characterized by thrust oscillations. From an examination of Fig. 11 in Ref. 9, these appear to be nearly regular with a period of approximately 16 s. The authors report this unsteady behavior might have been caused by vaporization of the flow within the valve before reaching the thruster. Through the Pyrex capillary they observed flow consisting of mostly vapor entering the chip. In addition, they determined that the vapor pressure at the measured valve temperature exceeded the inlet pressure, thereby enabling prevaporization.

If the flow rate were increased, the vaporization in the valve could be eliminated, but after some period of time, on the order of a minute, the chip temperature would drop to the point that the flow was only partially vaporized. This led to expulsion of some liquid water from the nozzle, which would freeze upon being exposed to vacuum. The authors identify a "sweet spot" of operation between these two modes, but could only sustain this "stable" operation for a limited time. In some cases, icing of the exiting flow was observed; in other cases the flow reverted back to an oscillatory mode.

The success of the VLM depends in large part on the ability to realize thrust-to-power (T/P) ratios comparable with other low-thrust options such as pulsed plasma thrusters with a T/P ratio of 15–20 μN/W at an efficiency of 10%. As an electrothermal thruster, it is essential that the thermal losses from the VLM be minimized. A well-known feature of two-phase flows is the phenomenon of dryout (alternatively referred to as burnout, boiling crisis, or critical heat flux). This is the point where most or all of the liquid has been vaporized and is characterized by a reduction in the heat-transfer coefficient, a rise in the wall temperature, and a slower rise in the vapor temperature. In the VLM, if burnout occurs too early in the heating process, then a significant fraction of the power will go into wall heating (leading to conduction losses) with only a modest increase in vapor temperature and specific impulse. This research seeks to investigate the phase transition in a VLM developed at the JPL with a Pyrex cover glass designed for optical access. The flow has been observed through a microscope and imaged with a digital video camera. Tests were performed at atmospheric pressure to measure the dryout point along the heated channel as a function of inlet flow rate and heater power. This paper describes the flow system hardware, calibration, video microscopy system, and initial characterization of the two-phase flow in the VLM.

Experiment Description

A specially made vaporizing liquid microthruster was fabricated at JPL for the purpose of imaging the two-phase flow within the microfabricated channel. Details of the VLM fabrication and initial thrust data are available in Ref. 9 and will not be repeated here. The primary difference between the VLM unit tested to date at JPL and the article provided for this work is that the upper silicon layer has been replaced by a Pyrex cover glass to provide optical access. The channel dimensions for the test chip are shown (not to scale) in Fig. 2, which represents a top view of the VLM. The fluid enters through an inlet on the left from below and flows along the channel over a gold film heater towards the converging-diverging nozzle on the right. Figure 1 shows a VLM test article from Ref. 9, which does not have Pyrex cover glass for imaging. The article shown is similar to the one tested in this work including the integrated valve and thermal standoff. A close-up of the nozzle throat is shown in Fig. 3.

Fluid Preparation and Flow Control System

All calibration tests described in this paper were performed with water. The mass flow-rate range of interest for this activity was 75–250 μg/s (0.27–0.90 g/h) and was chosen to include the flow-rate range over which thrust measurements have been obtained. A flow delivery system was assembled based on a similar design used at

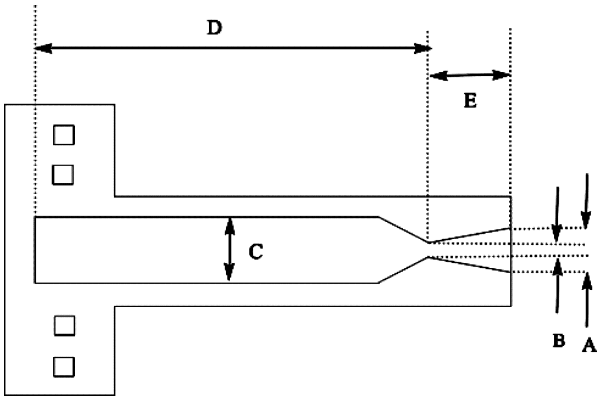

Fig. 2 VLM test model dimensions (top view, drawing not to scale): A = 618 μm, B = $\sim$62 μm, C = 709 μm, D = 7.8 mm, E = 1.1 mm, and depth = 300 μm.

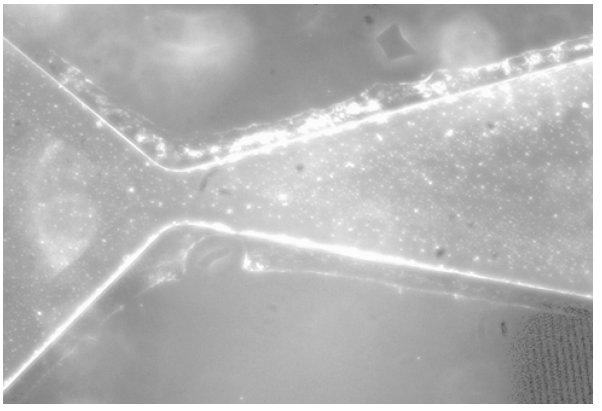

Fig. 3 Nozzle region of the VLM. Throat dimension is approximately 60 μm.

JPL in early vaporization tests. A schematic of the flow system is shown in Fig. 4. The water is stored in an electropolished stainless-steel sampling cylinder. The upper end of the cylinder is connected to a regulated air supply, which is used to inflate a balloon inserted into the cylinder. The expanding balloon allows for expulsion of the water without exposure of the water supply to pressurized air, which can increase the presence of dissolved gases in the water.

The water used was ultrapure spectrophotometric grade (Apha Aesar). Prior to filling the sample cylinder, the water was placed in a vacuum chamber, where the ambient pressure was reduced below the vapor pressure for a minimum of 10 min. This was done to facilitate the evolution and removal of any dissolved gases. The water prepared in this way was then either used to fill the sample cylinder or stored in a sealed bottle for future use.

The flow is passed first through a 10-μm filter and then a 2-μm filter before entering the capillary flow restriction. The control of such low flow rates required the use of a capillary to increase the pressure drop in the feed line. Approximately 25 cm of 63.5-μm i.d. (0.0025-in.) capillary made of polyetheretherketone (PEEK) was found to provide sufficient flow resistance. The pressure drop across the capillary was measured with a 50-psi (max) differential pressure transducer (Omega PX-2300). Two bleed valves were used to purge trapped air from the lines. The flow downstream of the capillary is fed to a length of ETFE (ethylene-tetrafluoroethylene) tubing with an i.d. of 0.040 in. (Upchurch Scientific), which was used to direct the flow into a bottle for the calibration as discussed next or to a barbed connector on the VLM device. A photograph of the flow delivery system is shown in Fig. 5.

Flow Calibration

The objective of the flow calibration was to determine the water flow rate as a function of the differential pressure across the capillary.

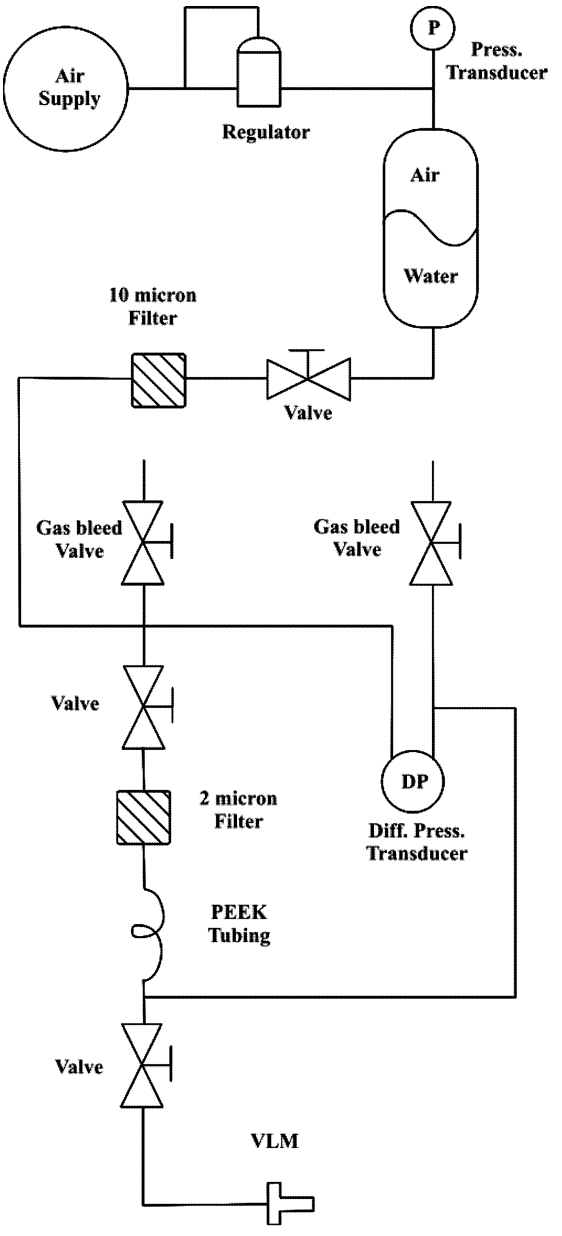

Fig. 4 Schematic of flow delivery system used for VLM testing.

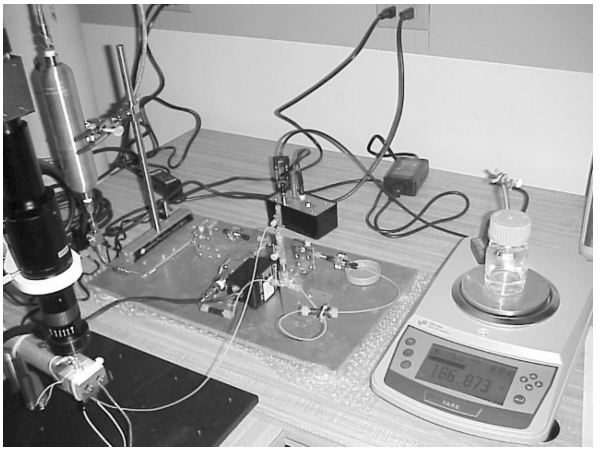

Fig. 5 Photograph of flow delivery system and balance used for calibration

Table 1 Calibration test data

Test	$\dot{m}$, μg/s	ΔP, psi	T, °C	$\Delta P_{0°C}$, psi	S, μg/s/psi[a]
FC5	81.35	7.58	22.8	14.24	5.71
FC4	121.35	11.53	22.9	21.67	5.60
FC3	182.02	17.08	23.4	32.50	5.60
FC2	205.58	19.65	22.9	36.89	5.57
FC1	232.91	23.27	21.2	41.98	5.55

[a]Average sensitivity coefficient was $S = 5.61 \pm 0.06$ μg/s/psi.

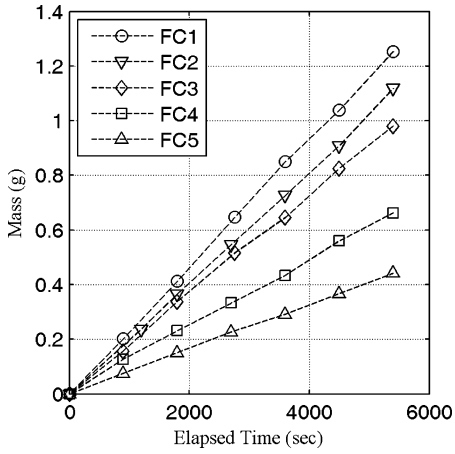

Fig. 6 Mass throughput vs time data used for flow calibration.

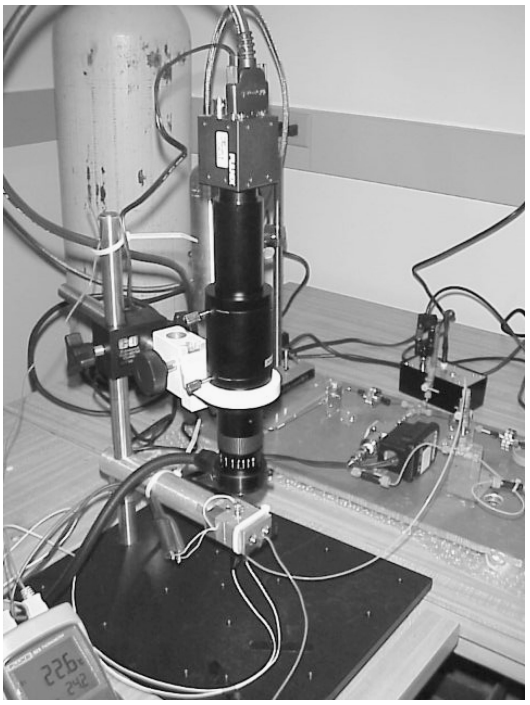

Fig. 7 Pulnix TM-1325 camera with VZM1000 lens used to image with VLM chip installed in mounting fixture.

This can in turn be used to determine a mass flow-rate sensitivity (g/sec/psi), which is normalized to a reference temperature.

The approach used involved weighing the water collected in a sample jar over a period of time. During calibration, the water is allowed to drip into a Pyrex bottle through a small hole in the lid. The hole is big enough to allow the ETFE tubing to be fed into the bottle without touching any surface but small enough to minimize evaporation of the water collected. The balance used was a Denver Scientific Pinnacle Series P-403 with a maximum capacity of 400 g and a resolution of 1 mg. Before testing, the balance was calibrated with an NIST traceable 100-g calibration mass (Denver Scientific "UltiMass" 0.15-mg tolerance on 100 g).

The data for the five calibration tests are shown in Fig. 6 and summarized in Table 1. The flow rates listed in column 2 of Table 1 correspond to the slope of the curves in Fig. 6. The third and fourth columns list the time average of the measured pressure drop across the capillary and ambient temperature respectively.

For laminar flow, the pressure drop will be proportional to a friction factor f as

$$\Delta P = f(L/D)(\rho V^2/2)$$

where L and D are the length and inner diameter of the tubing, ρ is the fluid density, and V the mean fluid velocity. The friction factor includes the viscosity dependence through the Reynolds number, which for a classical laminar flow is

$$f = 64/Re = 64\mu/\rho V D$$

Although the constant might be different in a particular experiment, the correction for the temperature dependence of viscosity only requires a recognition that $\Delta P \sim \mu$. The temperature dependence of viscosity for water is given by White[13] to within ±1%:

$$\ell_n(\mu/\mu_0) = -1.94 - 4.80(T_0/T) + 6.74(T_0/T)^2$$

where $T_0 = 273.16$ K and $\mu_0 = 0.001792$ kg/m/s. The next to last column in Table 1 lists the pressure drop after normalizing to T_0 to account for the temperature dependence of the viscosity.

Because the mass flow rate is proportional to the pressure drop, the ratio of these two quantities should be constant (after normalization to a reference temperature). These values are very nearly constant with an average value of $S = 5.61 \pm 0.06$ μg/s/psi. This sensitivity factor can be used to calculate the pressure drop required to obtain a desired flow rate when the viscosity correction is applied again, this time to correct for the actual ambient temperature.

Optical Imaging

Visual identification of the dryout point relies on the ability to distinguish a transition point in the two-phase flow within the channel. To accomplish this, a high-resolution monochrome progressive scan Pulnix-1325 camera was used. This camera has a 1392 (H) × 1040 (V) active pixel area with a charge-coupled-device cell size of 6.45 × 6.45 μm. The camera has a frame rate of 15 fps at full resolution and a electronic shutter speed of up to 1/16,000 second. The camera is connected to a National Instruments IMAQ PCI-1428 image capture board on PC with a 2.8 GHz Pentium 4 processor and 2 GB of RAM. The video microscopy system is shown in Fig. 7. The VLM is mounted under the lens in a custom made fixture allowing access to heater and valve electrical leads, thermocouple mounting and fluid supply.

Two lenses were selected for the initial set of studies. A VZM1000 zoom lens from Edmund Industrial Optics has a primary magnification range of 2.5–10. When used in conjunction with the 15-in. (38.1 cm) computer monitor, this allows a magnification of up to 500 X. The high-resolution image can be further digitally magnified to resolve features less than 5 μm in size. A second lens (Meiji UNIMAC Macrozoom) with a magnification range of 0.7–4.5 is used to image the entire channel in one image and for any application where a wider field of view is needed. A lens-mounted, ring fiber-optic illuminator is used to illuminate the VLM during imaging.

Results and Discussion

Bubble Nucleation

Initial investigations were performed to observe the transition of flow in the channel from single-phase liquid to full vapor. All images in this section were taken using the Meiji UNIMAC lens. For actual application as a thruster, the desired operational sequence would consist of initial heating of the dry channel before opening the valve to inject liquid. This was the sequence adopted in Ref. 9. To minimize the chance of burning out the heater in the test article

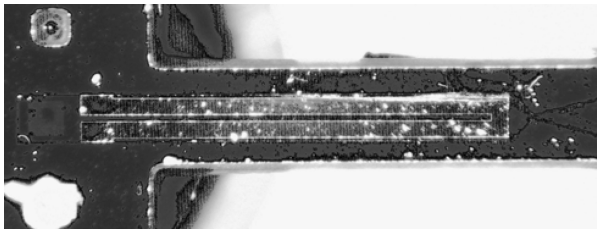

a)

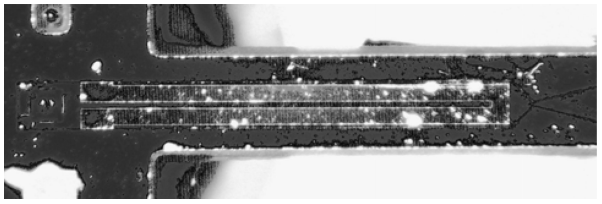

b)

Fig. 8 Image of channel with a) flow on, no heat and b) flow on, heater on (139 ± 1.6 μg/s, 0.55 W).

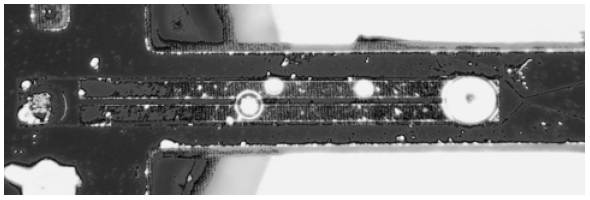

Fig. 9 Bubbles forming after unsteady ejection of vapor (139 ± 1.6 μg/s, 0.84 W).

available for this study, it was decided to initiate flow first without heating, and then gradually increase the heater power.

For a channel width of 700 μm and channel depth of 300 μm, the corresponding hydraulic diameter for the channel is 420 μm. For a mass flow rate of 200 μg/s, the corresponding Reynolds number is 0.71. At such a low Reynolds number one expects the vaporizing process to approximate that of pool boiling in which nucleate boiling is followed by a coalescence of bubbles into larger regions of vapor.

Figure 8a presents a baseline image with the flow turned on but without heater power. Defects in the Pyrex cover glass reflect light that appears as bright spots. In Fig. 8b three larger bright spots are visible near the channel exit. These are the first nucleation sites that became visible. Nucleation appears to begin along the outer edge of the heater channel, perhaps at locations where trapped gas or vapor pockets result in a higher local temperature.

Two-phase flow patterns specific to flow in microchannels have been studied by numerous researchers, and for a thorough review the reader is referred to Ref. 14. The regimes and their transitions can exhibit different characteristics than those observed in larger channels. As the bubbles in the VLM grow in size and multiply, they coalesce and form larger packets that eventually span the length of the channel. At no time were individual bubbles observed to separate from the surface and be carried downstream. The flow also did not appear to pass through an annular flow phase, although given the view through the coverglass onto the (opaque) heated surface the existence of such a phase could not be ruled out. In addition, condensation on the coverglass will tend to obscure what lies below. As will be discussed in the next section, these larger vapor packets appear to be periodically ejected. The channel then refills with liquid, and nucleation begins again. Figure 9 shows one of these nucleation cycles subsequent to ejection of a vapor packet. Flattening of bubbles is evident visually as concentric circles in the image as seen in the leftmost bubble in Fig. 9.

For these tests, the heater power was approximately 0.85 W, and the flow ranged from 135–175 μg/s. In this power and flow-rate range, the flow was observed to transition to a "pulsing" mode as described in the following section.

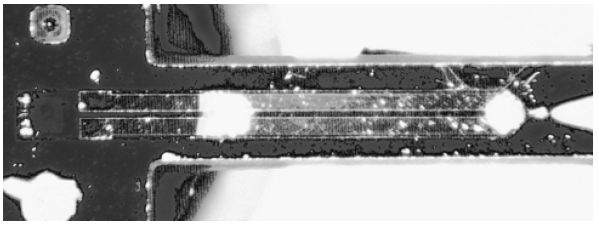

Fig. 10 Vapor packet between highly reflecting mist or condensation at extremes (139 ± 1.6 μg/s, 0.85 W).

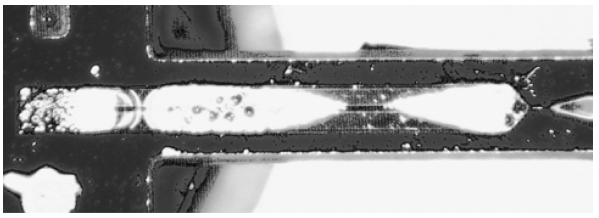

a)

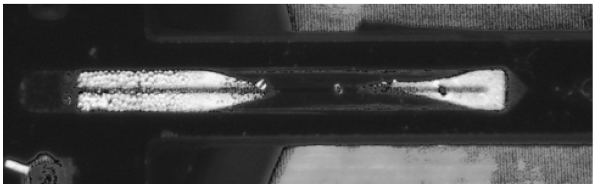

b)

Fig. 11 Image of channel during a) unsteady and rapid coalescing of vapor packets (139 ± 1.6 μg/s, 0.84 W) and b) later cycle imaged with reduced lighting (140 ± 1.7 μg/s, 0.83 W).

Unsteady Vaporization

After coalescing of individual bubbles, the vapor packet was observed to grow rapidly to fill channel and then begin a periodic contraction and expansion. One snapshot in this cycle is shown in Fig. 10. Vapor is transparent, but individual bubbles are highly reflective. In this image, the high reflectance of the flow through the nozzle suggests less than full vaporization. The bright regions likely indicate condensation on the inside surface of the Pyrex or fine droplets in the flow itself. A transparent (low reflection) region of nearly complete vapor is evident between the two bright areas.

In this mode of operation, pulsing was observed with approximately a 5-s period, in which the vapor packet would rapidly expand along length of channel. This expansion occurred such that the phase boundary moved towards the left from exit to inlet. In Fig. 11a, the vapor at the exit is seen as a bright area in the nozzle while the phase boundary is moving back toward inlet. The bright tear-drop shape is formed by condensed vapor on bottom of Pyrex. Between the tear-drop-shaped regions is nearly complete vapor.

Also in Fig. 11a, a large vapor packet is entering (at left) through the inlet to the channel as well. This could be a combination of gas and vapor although the clear feed tube to the VLM did not show any indication of air bubbles in the supply line during the test. A telling feature is the fact individual bubbles can be seen in the vapor packet at the inlet. The existence of these bubbles before the heater has been reached suggest boiling might have occurred in the valve as suggested in tests at JPL.[9] In Fig. 11b, the illumination has been reduced to more clearly show what is either nucleation on the bottom of channel or (more likely) condensation of vapor along top of channel (bottom of Pyrex). Pulsing appeared to be regular until interaction occurred with vapor entering from inlet.

The pulsing mode of operation just described appeared to be "stable" in the sense that after each pulse the two-phase boundary or dryout point would advance down the channel towards the exit and remain at approximately the same location until the next pulse. This dryout point (at the stable location) was measured at three different flow rates for a given power. These results are shown in

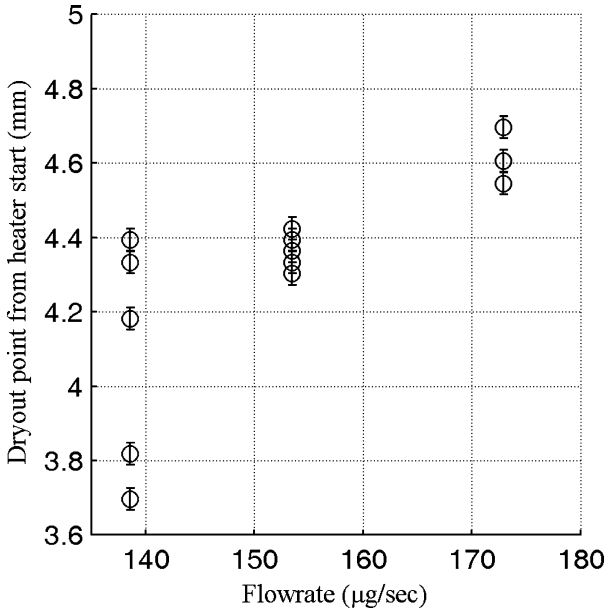

Fig. 12 Vapor boundary in channel during stable portion of pulsing cycle. Heater power is 0.83 W. Maximum uncertainty in flow rate is ± 2.0 μg/s.

Fig. 12. There are 5–6 separate measurements for each flow rate. The uncertainty estimate is the same for each data point and is based on the resolution of a scale used on the monitor to measure the location of the phase boundary. As one would expect, increasing the flow rate at a given power pushes the dryout point further down the channel towards the exit. Data colleted at the lowest flow rate are seen to exhibit the largest degree of scatter. This is believed to be a consequence of the fact that, in general, increases in pressure tend to reduce the sensitivity of void regions to disturbances[15] (the "spring constant" of the vapor region increases). Unfortunately, after data for the three flow rates in Fig. 12 were collected, the test device being used developed a leak, which resulted in most of the liquid flow being lost before reaching the channel, and so further tests to more fully map out this parameter space were not possible.

A number of phenomena can contribute to the onset of instabilities in two-phase flows. An extensive review of these mechanisms is presented by Tong and Tang.[15] They characterize dynamic instabilities as those in which "inertia and other feedback effects have an essential part in the process." These are in contrast to static instabilities in which a disturbance from a steady-state flow condition leads to a transition to a new steady-state condition markedly different from the original state. No conclusive identification of specific flow instability was made based on these tests. Nevertheless, from the movement of the dryout point upstream and the observed period (on the order of seconds), two possible candidates have been identified.

Thermal oscillations are a dynamic instability in which there is an oscillation between film boiling and transition boiling along the wall resulting in "large–amplitude temperature oscillations in the channel wall subject to constant heat flux."[15] This instability has been observed to cause fluctuation in the dryout point of steam-water mixtures. Tong and Tang classify these thermal oscillations as a compound dynamic instability because they require some disturbance to perturb the film boiling in the first place. One possibility for the destabilizing influence are density wave oscillations, another dynamic instability in which "temporary reduction of inlet flow in a heated channel increases the rate of enthalpy rise, thereby reducing the average density."[15] This change in density can alter the upstream pressure and heat-transfer characteristics and under certain conditions become self-sustaining.

A second possibility is the presence of pressure- drop oscillations that "occur in systems that have a compressible volume upstream of, or within, the heated section"[15] and have a characteristic frequency

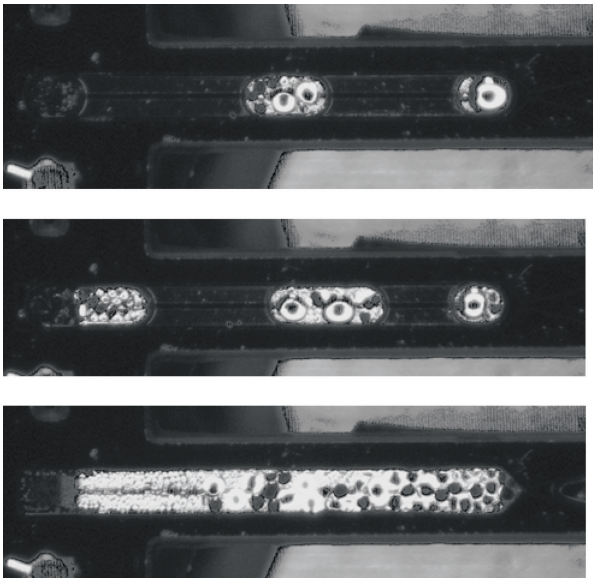

Fig. 13 Sequence of three images taken several seconds apart showing (in order) from top to bottom, multiple vapor packets coalescing (139 ± 1.6 μg/s, 0.84 W).

on the order of 0.1 Hz. In the case of the VLM tested, the presence of bubbles within or downstream of the valve provide a compressible volume upstream of the heating channel in the chip itself.

Vapor Packet Interaction

The pulsing mode described in the preceding section results in unsteady flow (and thrust as well). It is not clear at this point whether this pulsing is a result of pressure interactions with bubbles upstream, perhaps even within the valve itself. Attempts were made to view the interaction of the vapor packets specifically.

In Fig. 13, a sequence of three images is shown, which were taken less than 30 s apart. The illumination has been reduced so that the internal structure of individual bubbles in the vapor packet can be seen. In the top image, two packets are visible in the channel, but a packet within the passage to the inlet is as yet unseen. In the middle image, the packet is visible entering the channel.

It is believed to be a vapor bubble (because of the nucleation evident) but could be a gas bubble affecting the heat transfer locally. In the bottom image the packets have coalesced into a larger packet spanning the entire channel length. In this image, the heater starting point coincides with the boundary of the bright region. The variation in bubble sizes is very noticeable with bubbles increasing in size towards the exit. Movement of individual bubbles is not observed but rather the growth of the envelope of bubbles, which are coalescing.

Conclusions

A vaporizing liquid microthruster, specially fabricated to provide optical access, was used to study the two-phase flow in the microchannel with integral heater. Initial nucleation of bubbles in the channel as heater power is increased at a given flow rate was observed. Once full vaporization is achieved, the VLM was observed to operate in a stable, pulsed mode of operation with a phase front, which rapidly moves towards the inlet then recedes towards the exit to a repeatable location. In tests performed thus far, this pulsing had a period of approximately 5 s for flow rates in the range of 140–175 μg/s at a heater power of 0.85 W. This stable dryout point was measured as a function of flow rate at fixed power.

This pulsing mode of operation can be linked to interaction of vapor packets with vapor created upstream of the inlet, possibly in the valve. In addition, there is clearly an unsteady interaction that was observed when several vapor packets in the channel coalesce. Any of these complex interactions could adversely affect thrust stability as well as local heat-transfer rates and thermal efficiency.

Further study is warranted to determine if operation at higher inlet pressure can suppress some of the premature vaporization and

result in a nonpulsing and stable phase boundary or dryout point. Further analysis and measurements can then identify what regimes of power and flow rate can locate this dryout point optimally to maximize efficiency.

Acknowledgments

This work was supported in part by a grant from NASA. The authors would like to thank John Ziemer and Toshiro Hitake of the Jet Propulsion Laboratory for their assistance.

References

[1]Micci, M. M., and Ketsdever, A. D. (ed.), *Micropropulsion for Small Spacecraft, Progress in Astronautics and Aeronautics*, Vol. 187, AIAA, Reston, VA, 2000, Chaps. 3 and 8.

[2]Tilley, D. L., Pobst, J. A., Bromaghim, D. R., Myers, R. M., Cassady, R. J., Hoskins, W. A., Meckel, N. J., Blandino, J. J., Brinza, D. E., and Henry, M. D., "Advanced Pulsed Plasma Thruster Demonstration on MightySat Flight II.1," *Proceedings of the 10th AIAA/Utah State University Conference on Small Satellites*, AIAA, Reston, VA, Sept. 1996.

[3]Spanjers, G. G., Bromaghin, D., Lake, J., Dulligan, M., White, D., Schilling, J., Bushman, S., Antonsen, E., Keidar, M., and Boyd, I., "AFRL MicroPPT Development for Small Spacecraft Propulsion," AIAA Paper 2002-3974, July 2002.

[4]Blandino, J. J., Cassady, R. J, and Peterson, T. T., "Pulsed Plasma Thrusters for the New Millennium Interferometer (DS-3) Mission," International Electric Propulsion Conference, Paper IEPC 97-192, Aug. 1997.

[5]Blandino, J. J., and Cassady, R. J., "Propulsion Requirements and Options for the New Millennium Interferometer (DS-3) Mission," AIAA Paper 98-3331, July 1998.

[6]Cassady, R. J., Willey, M. J., Meckel, N. J., and Blandino, J. J., "Pulsed Plasma Thruster for the New Millennium Space Interferometer Experiment DS-3," AIAA Paper 98-3326, July 1998.

[7]Polzin, K. A., Choueiri, E. Y., Gurfil, P., and Kasdin, N. J., "Plasma Propulsion Options for Multiple Terrestrial Planet Finder Architectures," *Journal of Spacecraft and Rockets*, Vol. 39, No. 3, 2002, pp. 347–356.

[8]Arrington, L. A., Marrese, C. M., and Blandino, J. J., "Pulsed Plasma Thruster Plume Study: Symmetry and Impact on Spacecraft Surfaces," AIAA Paper 2000-3262, July 2000.

[9]Mueller, J., Ziemer, J., Green, A., and Bame, D., "Performance Characterization of the Vaporizing Liquid Microthruster (VLM)," International Electric Propulsion Conference, Paper IEPC 03-237, March 2003.

[10]Mukerjee, E. V., Wallace, A. P., Yan, K. Y., Howard, D. W., Smith, R. L., and Collins, S. D., "Vaporizing Liquid Microthruster," *Sensors and Actuators A*, Vol. 83, May 2000, pp. 231–236.

[11]Ye, X. Y., Tang, F., Ding, H. Q., and Zhou, Z. Y., "Study of a Vaporizing Water Micro-Thruster," *Sensors and Actuators A*, Vol. 89, No. 2, 2001, pp. 159–165.

[12]Maurya, D. K., Das, S., and Lahiri, S. K., "Silicon MEMS Vaporizing Liquid Microthruster with Internal Microheater," *Journal of Micromechanics and Microengineering*, Vol. 15, No. 5, 2005, pp. 966–970.

[13]White, F., *Fluid Mechanics*, 5th ed., McGraw–Hill, New York, 2003, p. 28.

[14]Ghiaasiaan, S. M., and Abdel-Khalik, S. I., "Two-Phase Flow in Microchannels," *Advances in Heat Transfer*, Vol. 34, edited by J. Hartnett, T. Irvine, Jr., Y. Cho, and G. Greene, Academic Press, San Diego, CA, 2001, pp. 145–254.

[15]Tong, L. S., and Tang, Y. S., *Boiling Heat Transfer and Two-Phase Flow*, 2nd ed., Series in Chemical and Mechanical Engineering, Taylor and Francis, Washington, DC, 1997, Chap. 6.